

UCRL-11485
c.2

University of California
Ernest O. Lawrence
Radiation Laboratory

AN ANALYSIS OF
 Υ^* PRODUCTION BY 1.15 BeV/c K^- BEAM

TWO-WEEK LOAN COPY

*This is a Library Circulating Copy
which may be borrowed for two weeks.
For a personal retention copy, call
Tech. Info. Division, Ext. 5545*

UCRL-11485
c.2

DISCLAIMER

This document was prepared as an account of work sponsored by the United States Government. While this document is believed to contain correct information, neither the United States Government nor any agency thereof, nor the Regents of the University of California, nor any of their employees, makes any warranty, express or implied, or assumes any legal responsibility for the accuracy, completeness, or usefulness of any information, apparatus, product, or process disclosed, or represents that its use would not infringe privately owned rights. Reference herein to any specific commercial product, process, or service by its trade name, trademark, manufacturer, or otherwise, does not necessarily constitute or imply its endorsement, recommendation, or favoring by the United States Government or any agency thereof, or the Regents of the University of California. The views and opinions of authors expressed herein do not necessarily state or reflect those of the United States Government or any agency thereof or the Regents of the University of California.

SPECIAL THESIS DIST.

UCRL-11485

UNIVERSITY OF CALIFORNIA
Lawrence Radiation Laboratory
Berkeley, California

AEC Contract No. W-7405-eng-48

AN ANALYSIS OF γ_1^* PRODUCTION BY 1.15 BeV/c K^- BEAM

Sun-Yiu Samuel Fung

(Ph. D. Thesis)

September 1963

Reproduced by the
Technical Information Division
directly from author's copy.

Contents

Abstract	iii
Introduction	1
Theory	3
Experimental Procedures	7
Data Analysis	12
Results and Conclusions	57
Acknowledgments	59
Reference	60

An Analysis of Y_1^* Production

by 1.15 BeV/c K^- Beam

Sun-Yiu Samuel Fung

(thesis)

Lawrence Radiation Laboratory
University of California
Berkeley, California

September 1963

ABSTRACT

The 30-inch propane bubble chamber⁽¹⁾ was used at the Bevatron to investigate Y_1^* production by 1.15 BeV/c K^- -meson interaction, $K^- + p \rightarrow Y_1^{*\pm} + \pi^\mp$, $Y_1^{*\pm} \rightarrow \Lambda + \pi^\pm$. The analysis was limited mainly to 548 events where the final state consists of a lambda hyperon and two pions of opposite charge, and which satisfy the hypothesis that the interaction took place in hydrogen.

Both the negative and the positive Y_1^* resonance states were observed. These decay strongly into a lambda hyperon and a pion. This Y_1^* state has a mass of 1378 ± 3 MeV, and a full-width at half maximum of 58 ± 6 MeV for the positively charged state, Y_1^{*+} and 70 ± 8 MeV for the negative one, Y_1^{*-} . The ratio of production cross-sections, $\sigma(K^- + p \rightarrow Y_1^{*-} + \pi^+)$ to $\sigma(K^- + p \rightarrow Y_1^{*+} + \pi^-)$, is 1.53 ± 0.16 . The cross-section for production of $\Lambda\pi^-\pi^+$ via Y_1^* is 2.33 ± 0.36 mb.

The production angular distributions were fitted to a power series in $\cos \theta_{\text{prod}}$, where θ_{prod} is the angle between the Y_1^* direction and that of the incoming K^- -meson in the center of mass of the K^- -p system. This distribution for the Y_1^{*+} system required a fourth order polynomial, while that for the Y_1^{*-} required a third order polynomial. Both imply that at least up to d-wave orbital

angular momentum states were present.

The spin state of the Y_1^* was studied via its various decay angular distributions. In particular, the Y_1^* decay angular distribution relative to the production normal, for Y_1^* production angles near 90° ($|\cos \theta_{\text{prod}}| < 0.5$), is not isotropic. This implies that the angular momentum of the Y_1^* state must be equal or greater than $3/2$.

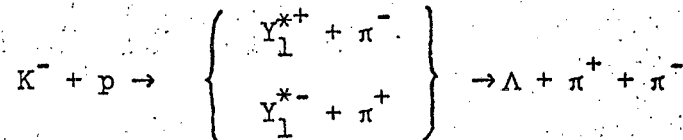
The forward-backward asymmetry of the proton in the lambda decay with respect to the production normal was studied in an attempt to establish whether the Y_1^* state is a p-state resonance, or a d-state resonance, assuming now the spin of the Y_1^* is $3/2$. In the former case, the Y_1^* - Λ parity would be even, while in the latter case, it would be odd. The results are not conclusive, although the data from Y_1^{*+} alone yielded a result slightly favoring the p-wave resonance, or the even parity case.

Introduction

In the fall of 1958 a high energy K^- beam was set up⁽²⁾ at the Berkeley Bevatron to search for the Ξ^0 hyperon. Both the 15-inch hydrogen bubble chamber and the 30-inch propane chamber were used for the investigation. Later, Alston et al.⁽³⁾ studied the reaction



in the hydrogen chamber, and found the π - Λ resonance state Y_1^* with mass 1385 MeV and half-width about 25 MeV. The reaction was interpreted as a two-step one in which the Y_1^* state is the intermediate π - Λ resonance state



This resonance state was predicted by Gell-Mann⁽⁴⁾ in his global symmetry scheme as a hyperonic analogue to the $(3, 3) N^*$ isobar resonance well known in π -N scattering. In this instance, the π - Λ resonance would be $P_{3/2}$.

This was also predicted by Dalitz⁽⁵⁾ as a bound s-state in the $\bar{K} N$ system which undergoes decay into the π - Λ channel. In this case, the Y_1^* state would have $J = 1/2$ and the π - Λ resonance would be in either the $S_{1/2}$ or $P_{1/2}$ state depending on whether the $K\Lambda$ parity were odd or even. Both of these theories are thoroughly discussed in references 4 and 5, so only a brief summary of the main conclusions will be presented in the next section.

Alston et al.'s investigation did not yield any conclusion with regard to the spin of the Y_1^* due to limited statistics. Therefore,

this study was undertaken with the 30-inch propane bubble chamber
film.

Theory

A. Global Symmetry with Doublet Approximation

The global symmetry model assumes that the strong couplings between pions and all of the baryons are of equal strength, and puts the baryons into doublets on the same footing as the (p, n) doublet. These strong couplings possess a high symmetry in baryons which is broken up by the weaker K couplings. Thus, the problem of pion hyperon interactions can be approximately reduced to a problem in the theory of pion nucleon interactions. In analogy to the $J = 3/2$, $T = 3/2$ π -N resonance, one would expect a similar pion-hyperon resonance. In the case of the Λ , a $J = 3/2$, $T = 1$ π - Λ resonance.

The mass and the width of this resonance can be obtained in an empirical way.⁽⁶⁾ One writes the isotopic spin \vec{T} as the sum of two terms, $\vec{T} = \vec{I} + \vec{K}$. \vec{I} is the spin that specifies the state completely in the global symmetry approximation in the absence of K couplings. \vec{K} is that part of isotopic spin due to the weaker coupling which breaks up this symmetry. Thus, for pions, $\vec{I} = 1$ and $\vec{K} = 0$; for kaons, $\vec{I} = 0$, and $\vec{K} = 1/2$. In this scheme, the Λ and the three charge components of the Σ form two doublets (Σ^+ , Y^0), (Z^0 , Σ^-) with $I = 1/2$ and $\vec{K} = 1/2$ where

$$Y^0 = \frac{\Lambda - \Sigma^0}{2} \quad Z^0 = \frac{\Lambda + \Sigma^0}{2}$$

Assume the phenomenological mass formulae

$$M = m(K^2) + \vec{I} \cdot \vec{K} \Delta$$

where $m(K^2)$ is the baryon mass dependent only on the K spin. For Λ , $\vec{I} \cdot \vec{K} = -1/4$ and for Σ , $\vec{I} \cdot \vec{K} = 3/4$; thus, Δ is the mass difference

of Σ and Λ , about 75 MeV and $m(K^2)$ is empirically found to be 1172 MeV for $K = 1/2$. For the Y_1^* resonance, one modifies the above empirical equation to the following form:

$$M = m(K^2) + I \cdot K \Delta + M_\pi + Q$$

where Q is the total available kinetic energy and is assumed to be the same as for the πN system. For Y_1^* , $T = 1$, $I = 3/2$, $K = 1/2$, and its mass is predicted to be about 1380 MeV.

The width of the resonance can be obtained from that of the corresponding pion-nucleon resonance, the $(3, 3)N^*$ resonance at 1238 MeV, with half-width $\Gamma / 2 = 45$ MeV. However, the Y_1^* resonance can decay through several channels. For example, the Y_1^{*+} can decompose into $\Lambda\pi^+$, $\Sigma^0\pi^+$, $\Sigma^+\pi^0$, the ratio of their amplitudes being $2/\sqrt{6} : 1/\sqrt{6} : 1/\sqrt{6}$. Thus, the width of the π - Λ resonance from the Y_1^* must be weighed by the I-spin factor $2/3$. Furthermore, due to the energy difference between the two resonances, the width is multiplied by a kinematic factor $(P_n^* / P_N^*)^{2\ell + 1}$, the momenta being measured in the center of mass frame of the appropriate resonance. For the Y_1^* , $P_\Lambda^* = 210$ MeV/c; for the N^* resonance, $P_N^* = 230$ MeV/c. The $(3, 3)$ resonance is dominated by the p-wave state, $\ell = 1$. Therefore, the full-width of the Y_1^* is predicted to be 46 MeV.

B. \bar{K} - N Bound-State Interpretation

Dalitz uses a zero-range approximation to treat the K-p collision with both elastic (\bar{K} -N scattering) and reaction (π -Y states) channels open. He shows that if the imaginary part of the scattering length b is small, i.e., the cross-channel interaction parameter is small, and if the real part is negative, then the \bar{K} -N system has an eigen-solution

$$\psi = \frac{1}{\sqrt{4\pi\mu_K|a|}} \frac{\exp(-r/|a|)}{r}$$

representing a $S_{1/2}$ \bar{K} -N bound state of mass

$$M = M_N + M_K - 1 / (2\mu_K a^2)$$

where μ_K denotes the \bar{K} -N reduced mass and a is the real part of the scattering length. However, this state is linked with energetically available π -Y channels, and there is a finite rate of transition from \bar{K} -N channel to the π -Y channels. This finite transition rate corresponds to a lifetime, with a half-width

$$1/2 \Gamma = \frac{b}{\mu_K |a|^3}$$

The resonance will be narrow if $|a|$ is large, or if b is small.

Using the data presented by Alvarez at Kiev⁽⁷⁾, $a = -1.08 \pm 0.2$

and $b = 0.20 \pm 0.06$, Dalitz obtained

$$M = 1382 \pm 20 \text{ MeV}$$

$$\Gamma/2 = 18 \text{ MeV}$$

The bound state model being the $S_{1/2}$ state, the Y_1^* resonance must also have spin one-half.

Recent analysis of low-energy K^-p data by Humphrey and Ross⁽⁸⁾ yielded two scattering-length solutions, neither of which, however, satisfied the requirements for a pion-hyperon resonance in the $T = 1$ channel below the K^-p threshold. However, this analysis is based on zero-effective-range theory, and cannot completely rule out the bound-state model interpretation.

Experimental Procedures

The K^- beam used in this experiment was designed by P. Eberhard et al.⁽²⁾. The layout is shown in Fig. 1. A spatial separation of the K mesons from the pion background was achieved through two stages of electromagnetic separation. A detailed description of the beam is given by P. Eberhard et al.⁽²⁾

During the run, a steady magnetic field of 13.5 kilogauss was maintained over the volume of the 30-inch propane bubble chamber. About 104,000 pairs of pictures, in stereo view, were taken. After rejecting pictures which had no beam tracks, which had one of the view missing, or which were of poor quality, 86,489 frames were usable. The beam momentum and the number of K^- per frame were determined as follows:

A. Beam Momentum

To determine the momentum of the K^- beam, 332 tracks were selected of length, L, greater than or equal to 10 cm, which satisfied the following criteria⁽⁹⁾:

1. They were all apparent K^- interactions
2. $\alpha = 90^\circ \pm 2^\circ$ *
3. $\beta = -6^\circ \pm 3^\circ$ *
4. The track must have passed through the thin window.

The coordinate system used to define α and β is shown in Fig. 2.

A scatter diagram of momentum versus x was made and it was found that, for track lengths less than about 19 cm, the distribution of points was very diffuse. So a further restriction that

* The angle was measured at $x = 3$ cm line, x is the coordinate measured lengthwise along the chamber, being defined to be 50 at the center of the chamber

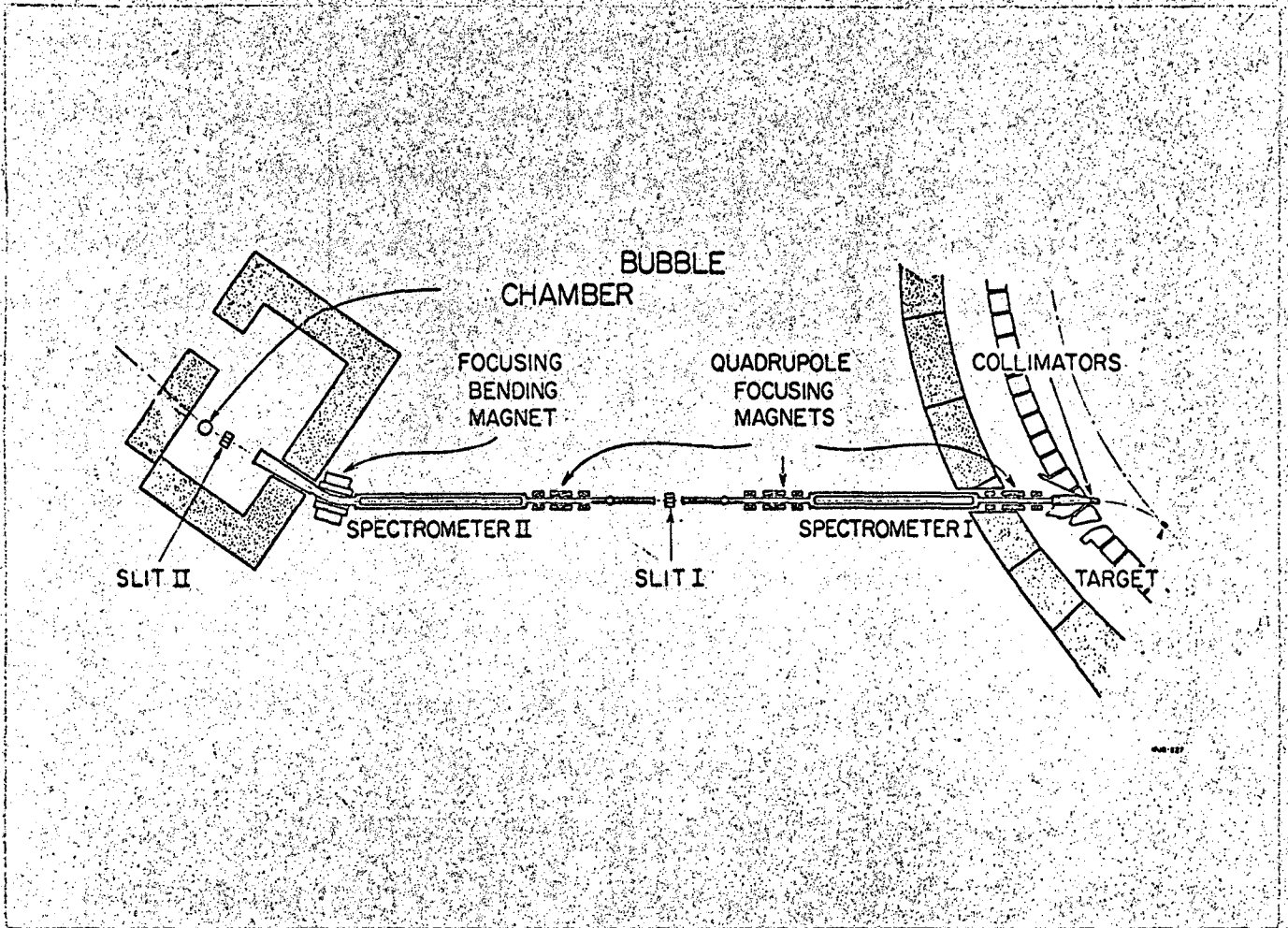
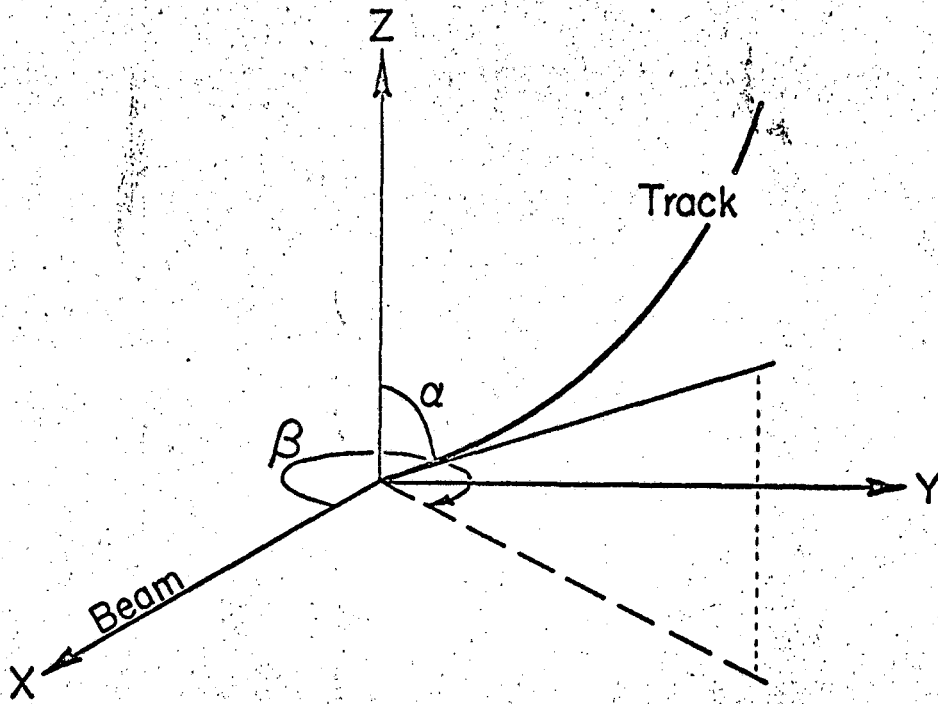


Fig. 1. The experiment layout of the separated K^- beam.



MU-18491

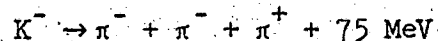
Fig. 2. The coordinate system used by FOG CLOUDY FAIR.

L must be equal to or greater than 19 cm was made and 264 tracks met this criterion. The momentum value was corrected for ionization loss and extrapolated to the center of the bubble chamber. The data were further divided into five subgroups according to their lengths. The mean of the momentum value and its standard deviation were found for each group. The final value was taken to be the weighted average of the five groups, which was found to be 1.104 ± 0.007 BeV/c at the center of the bubble chamber.

B. Estimation of Number of Tracks of K Particles

Two independent methods were employed to estimate the number of K particles:

1. By finding the number of τ decays where



In scanning 9237 frames of pictures, there were 127 decays which satisfied the τ decay hypothesis. Using the average momentum value of 1.104 BeV/c, with the mean life of K^- being $(1.224 \pm 0.013) \times 10^{-8}$ sec. and the branching ratio of K^- decaying into three charged pions being 5.66% ⁽¹⁰⁾, the number of K^- particles per frame is calculated to be $3.47 \pm .31$.

2. By finding the number of delta rays with kinetic energy greater than 5 MeV.

The cross-section for production delta rays of a certain minimum kinetic energy is a function of the velocity of the incoming particle. Thus, particles of different masses with the same momentum have different probabilities for producing delta-rays. At 1.1 BeV/c, the K^- particle cannot produce delta-rays of kinetic energy above 5 MeV. Any delta-ray above 5 MeV observed must be due to the

scattering either by a pion or a muon.

We counted 10,080 chamber lengths of track. If there were kinks on tracks, we measured their lengths up to the kinks only. The total number of delta-rays counted was 1,125 and there were 37 delta-rays on tracks before kinks.

For normalization, we counted the number of delta-rays and of kinks in a previous 30-inch propane bubble chamber run⁽¹¹⁾. The beam, consisting mainly of negative pions at 1.08 BeV/c, has $10 \pm 2\%$ muon contamination. For every hundred chamber-lengths observed, there were 24 delta-rays, and 26.6 kinks.

From the number of delta-rays counted in the two experiments, we computed the percentage of K^- in the beam to be $56.3 \pm 4.5\%$. From the number of delta-rays observed before kinks, we separated out the pion contamination from the muon contamination. The former is $(11.4 \pm 3.2)\%$, the latter is $(32.3 \pm 3.2)\%$.

The average number of beam tracks per picture was six. Thus, there were $3.38 \pm .27 K^-$ -meson per picture.

Results from these two independent methods agree well. For the computation of the cross-sections, the average of the two results, 3.42 ± 0.20 beam tracks per frame, was used.

Data Analysis

A. Scanning

The usable pictures were scanned specifically for neutral two-prong decays. These V particles were rejected if there were no possible beam tracks that could be interpreted as their production origins. If there were more than one possible origin, they were all noted on the scan cards. The scan cards guide the measurer to particular tracks that were of interest. These V particles could be either lambda decays, theta decays, or two-prong charged stars produced by neutron interactions. The scanner tried to classify the particles through kinematic identification curves⁽¹²⁾ and track ionization.

Only production origins which were associated with beam tracks were accepted. The restrictions on beam tracks were that the track must (1) have negative charge, (2) have minimum ionization, (3) come in through the upper end of the chamber, (4) have a curvature less than a certain value corresponding to some minimum momentum.

In 10,500 frames of pictures where the film is of the highest quality (between picture number 500 to 4,999 and 31,000 to 36,999), all production origins of V particles, regardless of the identity of the other secondary tracks, were accepted. For the rest of the film, only those V particles which satisfied the following criterion were accepted: their production origins must not have more than two charged secondary tracks, one of which must be a negative pion.

The accepted events were then measured on either a digitized microscope or a "Frankenstein". The latter is a motor-driven microscope with a servo-mechanism which centers automatically on the track. A track was measured by determining the location of a series

of points along it with respect to fiducial marks in both views. The resulting data were processed by the FOG CLOUDY FAIR system⁽¹³⁾.

The bulk of the film was scanned by a professional scanner. Out of 86,498 frames, 10,000 frames were double scanned by the scanner and the writer to determine the former's scanning efficiency, which was found to be 85.9%.

In this experiment, there were 2,442 events which were candidates of the type of interaction



It was not always possible to identify a positively charged secondary which could be either a positive pion or a proton. At the production origin, the presence of the proton would mean the interaction had taken place in carbon; at the decay origin, the ambiguity implied the V particle could be either a lambda decay, a theta decay, or a neutron interaction. In any case, provisions were made for different permutations of masses for the ambiguous track so that decisions could be made later after precise measurements were made. Events were rejected if the ambiguity persisted after constraints.

B. Data Reduction

A detailed description of the FOG CLOUDY FAIR system is given in reference 12. So only a brief summary will be attempted here.

FOG reconstructs the spatial position of each track, finding the dip angle, α , and the azimuthal angle β , and obtains the momentum through curve-fitting the track projected onto a plane parallel to the bottom of the chamber. It also applies a series of checks on the measurement input for errors that might have been

made during measurement.

CLOUDY calculates the errors on angles α and β and momentum for each track. It applies kinematic constraints, by adjusting parameter, X_i , through successive iterations until the quantities F_λ 's are zero and M is minimized. These quantities are defined as follows:

$$M(X_i, \alpha_\lambda) = \sum_{i=1} \frac{(X_i - X_i^m)^2}{\Delta_i^2} - 2 \sum_{\lambda=1}^4 \alpha_\lambda F_\lambda(X_i)$$

where X_i^m is the actual measured value of X_i

Δ_i is the error on X_i

α_λ are the Lagrangian multipliers introduced

F_λ are the four constraint equations for forward momentum, transverse momentum, coplanarity and total energy at an origin.

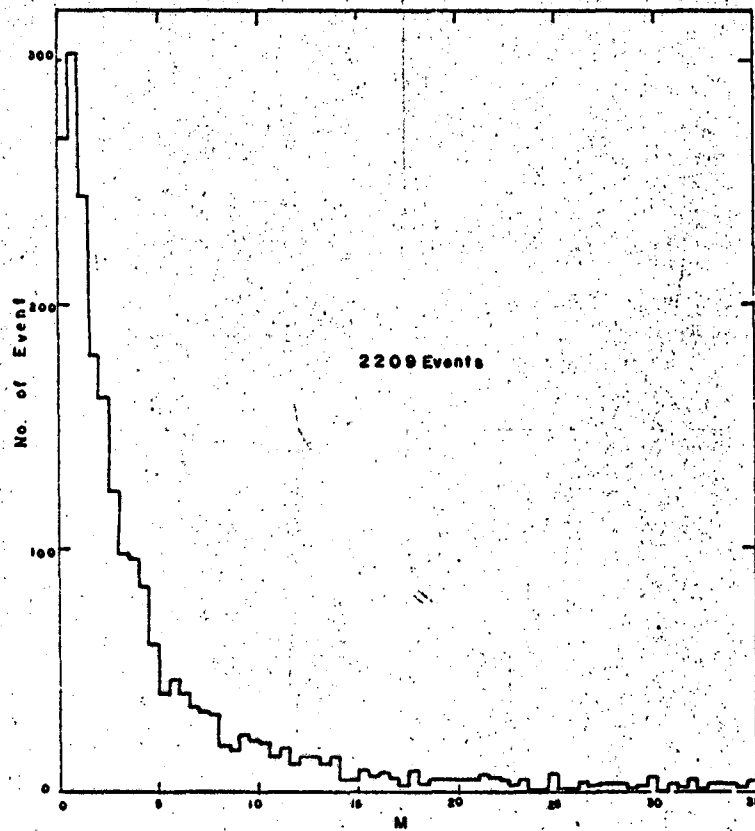
The program also performs a center-of-mass transformation and calculates the Q-value between any two tracks.

FAIR organizes the result of the computations and presents the output data in various forms.

C. Constraint of Lambda

Energy and momentum conservation gives four constraining equations. In the case of lambdas, one quantity is not directly measureable, namely, the momentum of the neutral (incoming) track of the V-particle. Thus, there are only $4 - 1 = 3$ degrees of freedom. For each event, the quantity M , which is equivalent to Chi-square when all the F 's are constrained to be zero, was computed.

Fig. 3 shows the distribution of M for V-particles which have two



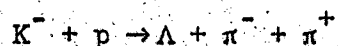
MU-31650

Fig. 3. Histogram of M for lambda decays. The cut-off was set at $M = 10$.

pions of opposite charges at their production origins. It is very similar in shape to that of theoretical Chi-square distribution, peaking at about one. However, it has a broader tail and there are too many events with lower M values. A cut-off of $M \leq 10$ was chosen, i.e., only V particles with $M \leq 10$ were accepted. 1,927 out of 2,442 events satisfied this criterion. The ambiguous events which fitted both the lambda and the theta constraints, with M less than 10.0, were rejected in the subsequent analysis. About 14% of the events were omitted in this way.

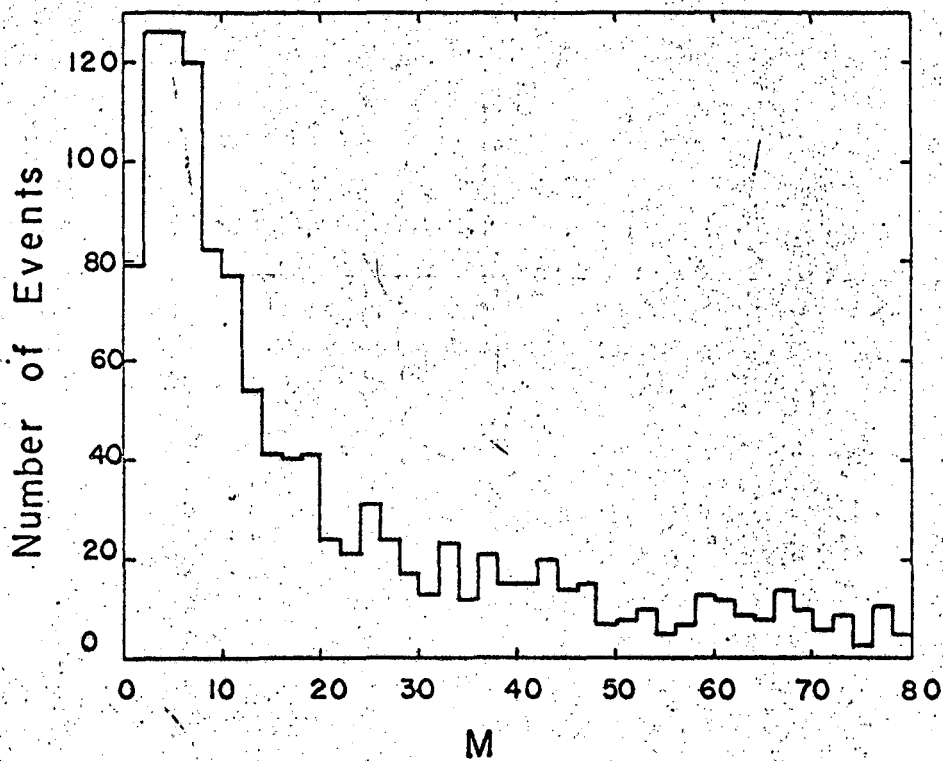
D. Constraint of Interactions at Production Origins

With the calculated values of p , d' , β for each lambda, the event was constrained at the production origin to be from the following interaction



Since quite often the K^- track was too short for accurate measurement, the momentum from investigation of long incoming tracks was better known, the edited momentum of 1.11 ± 0.3 BeV/c was employed for the incoming beam. This range is quite adequate; for at this momentum, the ionization loss in propane is about 1.1 MeV/c. Again, one has four constraining equations, but all quantities are now known. There are four degrees of freedom. The resulting M distribution is shown in Fig. 4. It peaks around $M = 5$ and does not vanish at high M values. There appears to exist a constant background of 10 events per interval, each interval having a width of $\Delta M = 2$.

The "probability paper"⁽¹⁴⁾ was used to determine how well the M distribution fitted a theoretical chi-squared distribution. On



MU-31652

Fig. 4. Histogram of M for hydrogen-like interaction. The cut-off was set at $M = 12$.

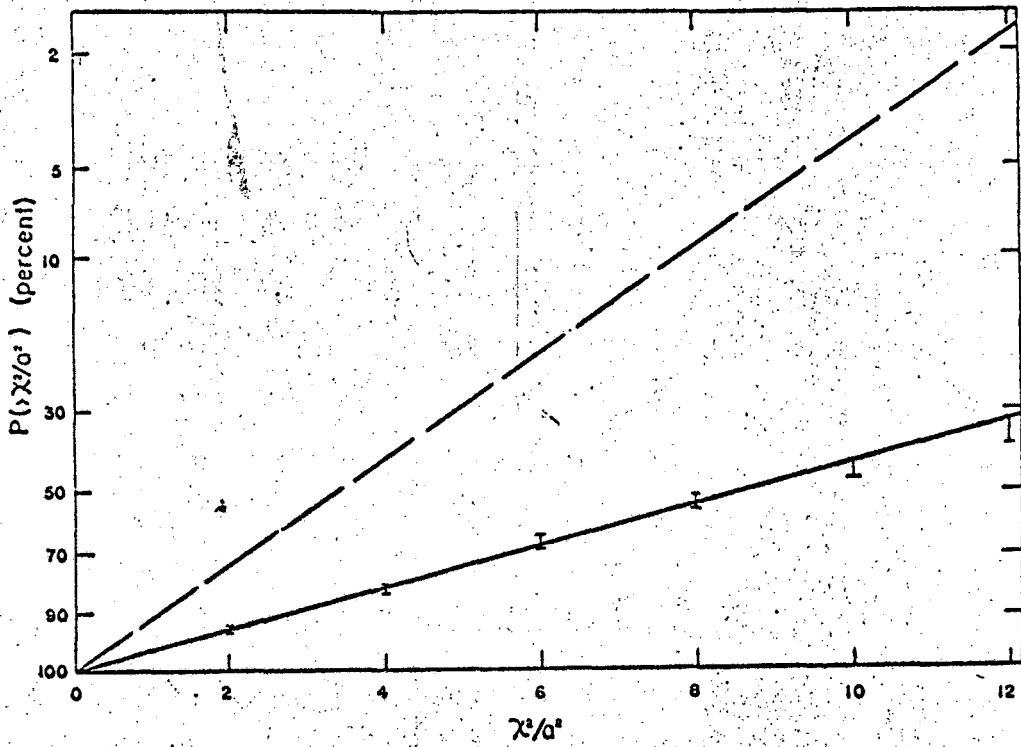
the "probability paper", values of χ^2/a^2 are plotted linearly along the abscissa; along the ordinates, there is also a linear scale in χ^2/a^2 , but the points are labelled instead with corresponding values of $P(>\chi^2/a^2)$. χ^2 is the chi-square value. "a" is a variable parameter, associated with input errors. $P(>\chi^2/a^2)$ is the integral chi-squared distribution corresponding to the fraction of total number of events, in percentage, with a value χ^2/a^2 or greater.

$$P(>\chi^2/a^2) = \int_{\chi^2/a^2}^{\infty} f(\chi^2/a^2) d(\chi^2/a^2)$$

where $f(\chi^2/a^2)$ is the theoretical χ^2 distribution. If the M distribution behaves in general like a chi-squared distribution, the plot of $P(>M)$ vs M would be a straight line. $P(>M')$ is the fraction of the events with M equal to M' or greater. Furthermore, for correct input errors, the plot would coincide with the dotted line shown in Fig. 5. The dotted line corresponds to $a = 1$.

After subtracting the background, we computed the percentage of events with M equal to or greater than certain values and the results are shown in Fig. 5. The points fall on a straight line, lying to the right of the dotted line. This shows that the M distribution behaves like a chi-square distribution, but that the estimated input error was too small. The cut-off of $M = 12$ was selected and would include 10% background. There were 611 such events. From Fig. 5 it is seen that this cut-off $M = 12$ corresponds to a χ^2 of 4.9 and that about 32% of the good events are excluded. In the computation of the total cross-section, this was one of the necessary corrections.

In the following analysis, the restrictions that $M \leq 12$ for constraining at the production origin and that $M \leq 10$ at the decay



MU.31642

Fig. 5. $P(M)$ versus M . $P(M)$ is the fraction of total number of events, in percentage, with a value M or greater.

origin were imposed. There were 548 events satisfying these criteria.

E. Analysis of Data

The Existence of the Y_1^* Resonance

The existence of a resonance can be shown by either a direct scattering experiment at numerous energies and the observation of a prominent peak in the total cross-section at the total energy corresponding to the mass of the resonance, or a production experiment where the decay products of the resonance are seen and the observation of a prominent peak in the invariant mass between the decay products. The latter method was suitable for the present experiment.

In the reaction



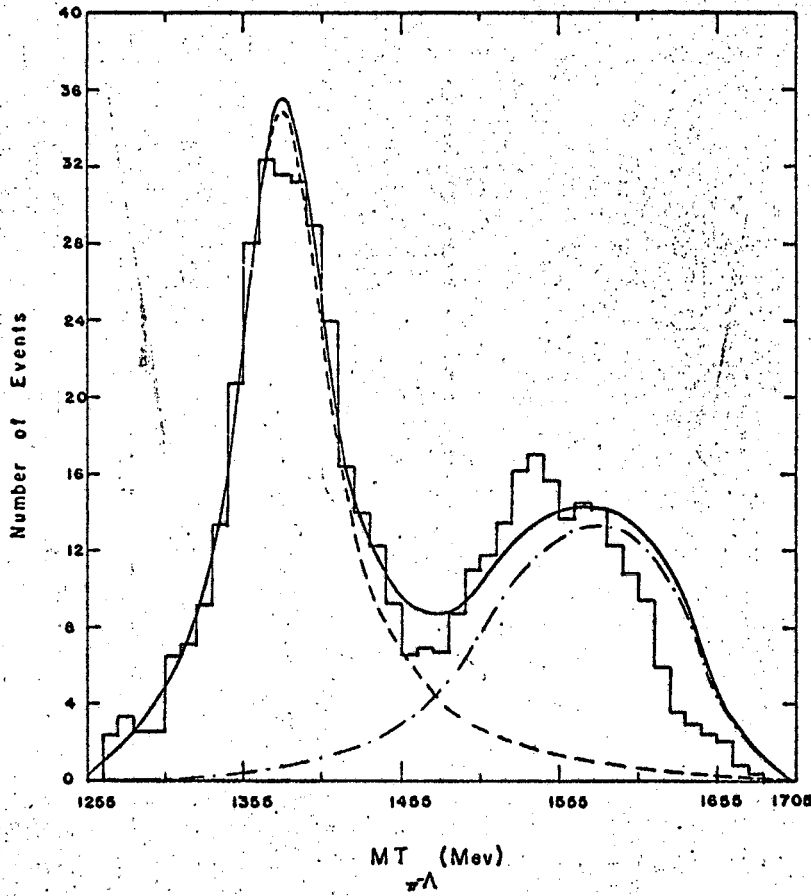
the invariant mass M between the lambda and one of the two pions produced was computed.

$$M(\Lambda, \pi) = \left((E_\Lambda + E_\pi)^2 - (\vec{P}_\Lambda + \vec{P}_\pi)^2 \right)^{1/2}$$

All quantities were measured in the laboratory system, since the invariant mass M is a constant regardless of the frame of reference.

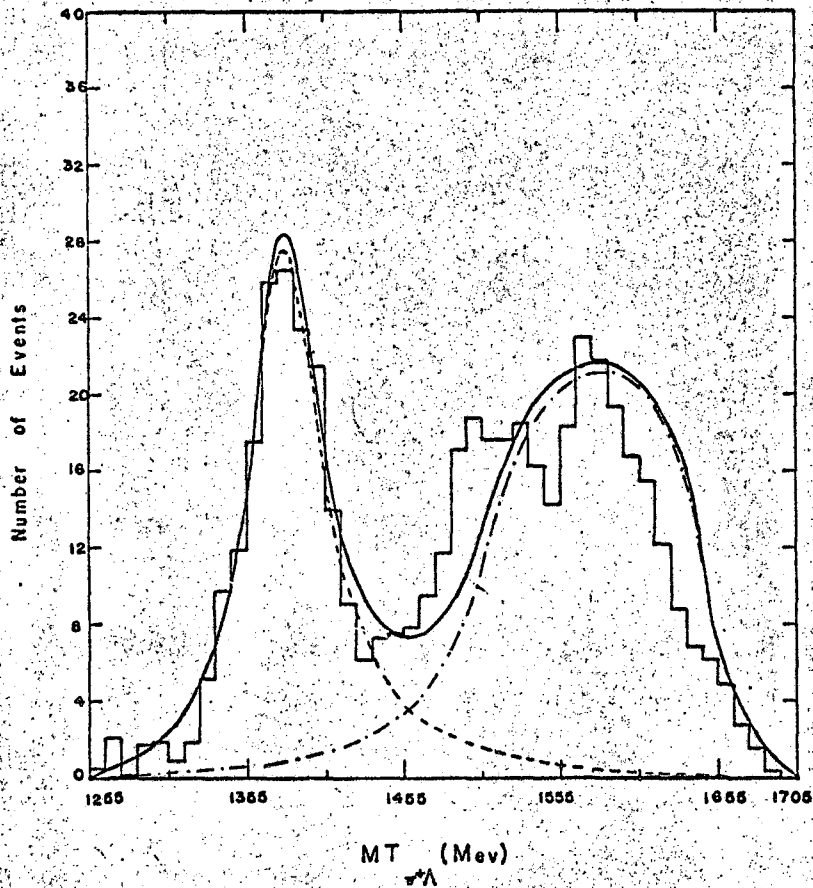
In Figures 6 and 7 are plotted the invariant masses between the lambda, the positive pion, and the negative pion respectively. In the plotting, each event was represented by a Gaussian of unit area where the central value was given by M and the standard deviation by dM , the uncertainty in M .

In each diagram, there are two peaks: a narrow peak about $M = 1378$ MeV and a broader peak at higher energy. The first peaks are to be interpreted as due to the formation of Y_1^{*+} and Y_1^{*-} resonance, which subsequently decay into a lambda hyperon, a positive pion and



MU-31644

Fig. 6. Histogram of $M(\Lambda^-, \pi^-)$, the invariant mass between lambda and the negative pion, in Bev.



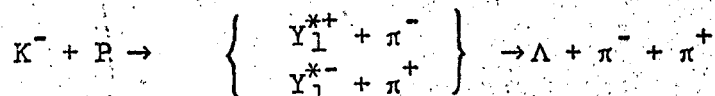
MU.31643

Fig. 7. Histogram of $M(\Lambda^+, \pi)$, the invariant mass between lambda and the positive pion, in Bev.

a negative pion respectively. The second peaks are the reflections of the resonance peaks due to kinematics. For example, in the $M(\Lambda, \pi^+)$ distribution, the contribution to the broader peak was from events which lay under the resonance peak in the $M(\Lambda, \pi^-)$ distribution. The interaction



is a two step process where



The distributions, for $1345 \text{ MeV}/c \leq M \leq 1425 \text{ MeV}/c$, were fitted with theoretical three-body Lorentz Invariant phase space distributions, with the assumption that a resonance occurs between the lambda and the pion. The resonance is represented by a factor of the form⁽¹⁵⁾

$$\frac{N}{(M - M_0)^2 + (\Gamma/2)^2}$$

where M_0 is the mass of the resonance, Γ is the full width of the resonance at half the maximum amplitude, and N is a normalization factor.

The dashed lines represent the best fitted resonance curves and the dotted curves represent the expected value of M when the other pion is resonating with the lambda, i.e., in the M distribution of Λ and π^+ , the π^- is the resonating particle. The solid lines are the sum of these two curves. The best value of M_0 and $\Gamma/2$ are tabulated in Table I.

To show that the peak in the $M(\Lambda, \pi)$ distribution is not due to a resonance of the pions*, the Dalitz plot where the kinetic

* The threshold for the ρ two-pion resonance is 1880 MeV; the energy of the present experiment is 1865 MeV.

TABLE I

Central mass value M_0 and half-width $\Gamma/2$ of Y_1^* , in MeV

Resonance State	M_0	$\Gamma/2$
Y_1^{*+}	1378 ± 3	29 ± 3
Y_1^{*-}	1378 ± 3	35 ± 4

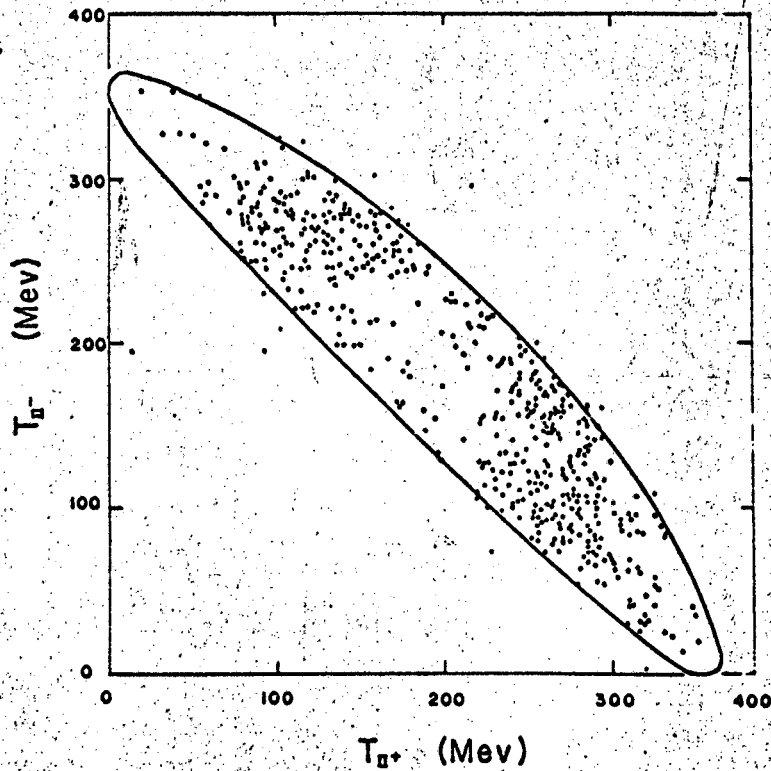


Fig. 8. Dalitz plot of kinetic energies of the two pions, in the K^-p center of mass, in Mev.

energies of the two pions, T_{π^-} and T_{π^+} , in the reaction center of mass, are plotted as shown in Fig. 8.

The Dalitz plot has the property that unit area $dT_{\pi^-} \times dT_{\pi^+}$ is just proportional to the element of volume in phase space ⁽⁶⁾. Thus, if individual events are plotted in the T_{π^-} - T_{π^+} plane, the density of events is proportional to the square of the decay matrix element. If there is no interference between the two pions in the final state, the points representing the events should spread uniformly over the entire plane within a confined region due to the constraint of conservation of energy and of momentum. The presence of a two-pion resonance would result in a cluster of data about a line with slope equal to -1, its exact position depending on the mass of the two-pion resonance. This was not observed.

Instead, there were two bands of points, one horizontal and one vertical. This agrees well with the interpretation that the production was a two-body final state process. While one pion is produced together with the hyperon, in the form of a Y_1^* , the other pion carries a unique amount of kinetic energy. The resonating pion shares the energy with the lambda, thus it can have various values for its kinetic energy, resulting in a line associated with a unique T_{π} of the non-resonating pion. But, from the data, the Y_1^* is a resonance having finite width, thus the kinetic energy of the non-resonating pion also has a range, and the line becomes a finite band.

The relation between the pion kinetic energy and Y_1^* mass is

$$\frac{dM_{Y^*}}{dT_{\pi}} = - \frac{E}{M_{Y^*}}$$

For a mass of 1380 ± 30 MeV, the full band width is 44 MeV.

For the subsequent analysis, only events with invariant mass M lying between 1305 and 1445 MeV were used. Analyses were also carried out with a narrower range of M , in particular, for $1345 \leq M \leq 1425$ MeV. The results obtained for these two ranges of invariant masses cut-off agree. In the following discussion, the broader cut-off, $1305 \leq M \leq 1445$ MeV, was used.

Production Cross-section

Between the limits of invariant mass, 1305 MeV and 1445 MeV, there are 238 events with $M(\Lambda, \pi^-) > M(\Lambda, \pi^+)$ and 156 events with $M(\Lambda, \pi^-) < M(\Lambda, \pi^+)$. Therefore,

$$\frac{\sigma(K^- + p \rightarrow Y_1^{*-} + \pi^+)}{\sigma(K^+ + p \rightarrow Y_1^{*+} + \pi^-)} = 1.53 \pm .16$$

No corrections need to be made, for presumably the same bias are present identically in both Y_1^{*-} and Y_1^{*+} channels.

To find the absolute cross-section for reaction $K^- + p \rightarrow \Lambda + \pi^- + \pi^+$ via Y_1^* production, several criteria and bias corrections must be taken into consideration:

1. Because of the uncertainty in interpreting the chi-square distribution for the constraint of lambda decay; for the purpose of computing cross-section, only the cut in chi-square value for hydrogen-production constraint was used, i.e., only events with $\chi^2 \leq 4.9$ were accepted. There were, as seen on page 18, 611 such events. Out of these was 10% background, which were due to carbon events where a production on a proton bound in carbon may simulate a production from a free proton. In Fig. 5, it is seen that, for a cut at $M = 12$ or $\chi^2 = 4.9$, 32% of good hydrogen-production events lie beyond this cut. An uncertainty of $\pm 6.25\%$ was estimated for this correction to allow for some variation of the fitted straight line.

2. In order to determine the fraction of events missed in the process of scanning, we computed the scanning efficiency of each scanner. To evaluate the efficiency of scanner A, a portion of films scanned by A was rescanned independently by scanner B.

The scanning efficiency of A is then expressed by

$$e_A = \frac{N_{AB}}{N_{AB} + n_B}$$

where N_{AB} = number of events both A and B found

n_B = number of events which only B found.

Assuming that A's scanning efficiency was constant, the corrected number of events found by A should be N_A/e_A , where N_A is the number of events found by A.

The average scanning efficiency was then found to be $86 \pm 3\%$.

3. There are two non-leptonic decay modes for lambda



The neutral decay (B) is difficult to detect. It is known that the ratio of charged (A) to neutral decay is approximately two to one. Since only the charged mode was observed in the scanning, a correction factor of $1.56 \pm .07^{(17)}$ was multiplied to the observed number of hydrogen-productions.

4. For the convenience of computing path length and of measuring the decay secondaries, a fiducial volume at reasonable distance inwards from the walls of the physical chamber was chosen.

This chosen volume excluded 2 cm each at the bottom end and at the top of the chamber, 8 cm on each side in the transverse direction, 8 cm on the front side where the beam entered, and 18 cm on the opposite end.

Both the production and the decay origins were required to be inside this volume.

5. Azimuthal angle (ϕ) bias occurred when the decay plane of

lambda was nearly vertical and the decay secondary tracks became too short to be detected and/or measured. The normal of the decay plane is defined by the vector, $\underline{p}_p \times \underline{p}_\pi$, where \underline{p}_a denotes unit vector momentum of particle a.

This bias was corrected by investigating the azimuthal angle distribution of the outgoing track about the incoming track, which would be isotropic if there were no missing events. There were two azimuthal angles to be examined: the one made by the lambda about the incoming K^- track, $\phi_{\Delta K}$, and the other made by the proton from the lambda decay about the lambda direction, $\phi_{p\Lambda}$.

The two distributions are shown in Figs. 9 and 10, and are consistent with isotropic distributions. Thus, we consider the correction to be nil, but estimated an error of 2% to the correction.

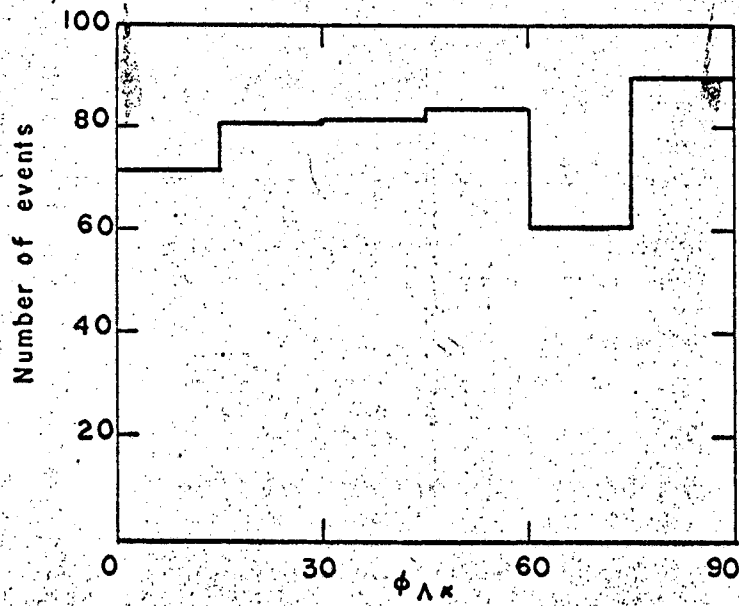
6. Lambdas which decayed too close to or too far away from the production origins were missed in scanning. Since lambdas exhibit an exponential decay, we found N_0 , the true number of lambdas produced, by the following expression:

$$n_1 - n_2 = N_0 \left(\exp \left(-\left(\frac{L}{P}\right)_1 \frac{K}{\tau} \right) - \exp \left(-\left(\frac{L}{P}\right)_2 \frac{K}{\tau} \right) \right)$$

where n_1 is the number of lambdas which survive after a time $K\left(\frac{L}{P}\right)_1$, τ is the mean life of the lambda, and K is 0.372×10^{-10} BeV-sec/cm when L is expressed in cm, p in BeV/c and τ in sec.

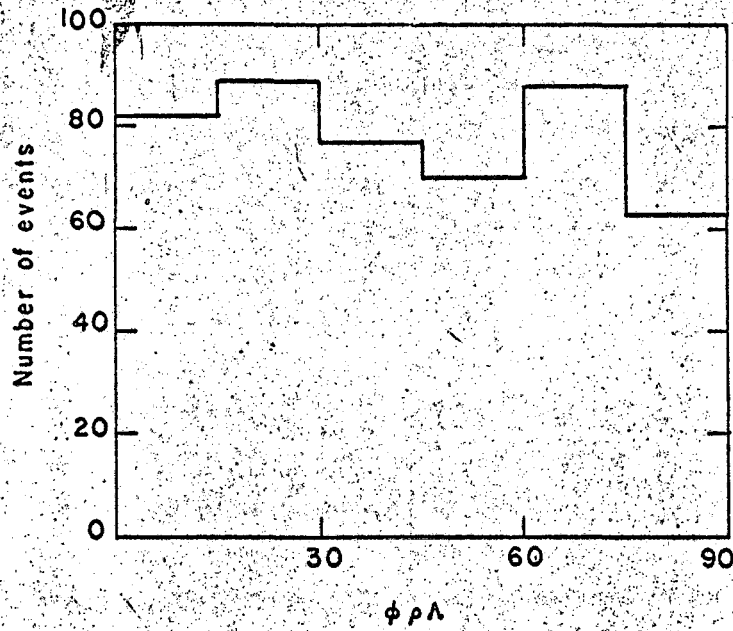
Thus, $n_1 - n_2$ is equal to the number of lambdas observed to decay between the time interval $K\left(\frac{L}{P}\right)_1$ and $K\left(\frac{L}{P}\right)_2$.

In order to find N_0 , we assumed that between the interval $1 < L/P < 8$ cm/ (BeV/c) all events were observed. The validity of this assumption was supported by the fact that the distributions



MU-31655

Fig. 9. Distribution of the azimuthal angle of lambda about the incoming K beam direction.



MU-31656

Fig. 10. Distribution of the azimuthal angle of proton about the lambda direction.

of L/P between the interval $(L/P)_1 = 1$ and $(L/P)_2 = 8$ are identical, with or without the criterion that the distance transversed by lambdas L must be greater than 0.5 cm and less than 24 cm.

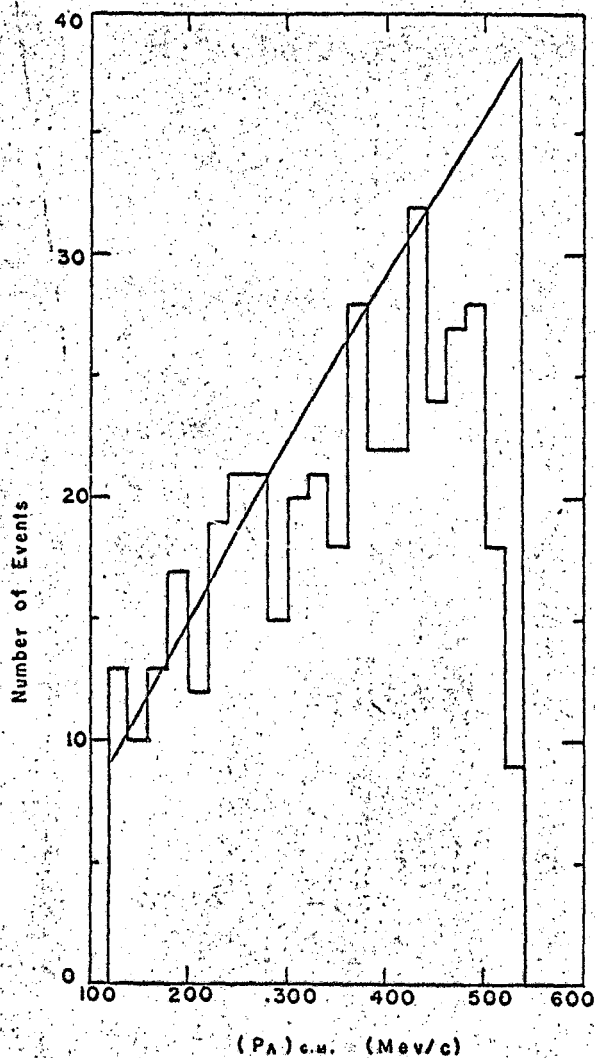
We used a value of $2.69 \pm 0.13 \times 10^{-10}$ sec. for the mean life of the lambda, as previously determined from this experiment⁽¹⁸⁾, and found that between $L/p = 1$ and $L/p = 8$ lies $46.0 \pm 6.3\%$ of the total number of events. Thus, we can correct for the events with extremely short or long lines of flight.

7. Lambda decays would escape detection if the secondary proton was too short to be visible. For a proton of momentum 110 MeV/c, which would be approximately 1 mm in length in propane, the maximum momentum for the lambda is 250 MeV/c. Thus, these "one-prong" lambdas were slow ones. They were produced backward in the center of mass of the K^-p system. As will be shown later, Y_1^* 's were produced mainly backwards also. Therefore, these slow lambdas were those which were produced forward with respect to the Y_1^* direction in the Y_1^* center of mass.

To correct for these invisible lambdas, the distribution of lambda momenta in the center-of-mass of the K^-p system was compared with its theoretical distribution. Assuming that the lambdas decay isotropically in the Y_1^* center-of-mass system, the energy distribution, $n(E^*)$ of the lambdas in the center-of-mass of the K^-p system will be flat. The momentum distribution, $n'(p^*)$, is related by

$$n'(p^*) = n(E^*) p^*/E^*$$

This is represented by a smooth curve in Fig. 11, the lower and upper sharp cut-offs correspond to lambdas decaying directly backward and forward respectively in the center-of-mass of the Y_1^* .



MU-31657

Fig. 11. Distribution of momenta of lambda from Y_1^* , in the K^-p center of mass. The solid curve is the theoretical distribution, normalized to the number of events for $120 \leq P_{\Lambda}^* \leq 300 \text{ Mev/c}$.

with $1 \leq L/p \leq 8$ cm (BeV/c), there are 249 events. After applying all the corrections, the number of interactions is estimated at 1104 ± 138 .

TABLE II

Corrections to the data expressed in percentage

Scanning efficiency	85.9 ± 3.0
Good event beyond $M = 12$	47.1 ± 4.1
Neutral decay mode	56.0 ± 7.0
Azimuthal angle	0.0 ± 2.0
$1 \leq L/p \leq 8$	85.2 ± 11.7
One-prong lambdas	16.3 ± 9.8
Rejects	2.1 ± 1.0
Σ^0 contamination	87.5 ± 2.5

Normalization of Beam Path

To convert the (corrected) observed number of events to a cross-section value, the total beam path length must be known. Since only events with $25 \leq x \leq 65$ cm were included in the cross-section calculation, the interaction volume is 40 cm long. Not all tracks which enter the interaction volume traverse its entire length, due to interaction. Let l be the interaction volume length, λ be the mean-free path for all interactions in the propane, then the average length a track goes before interaction is

$$L = \lambda (1 - \exp (-l/\lambda))$$

The mean-free path used was computed from K^- -p and K^- -n total cross-sections⁽¹⁹⁾ to be on the order of 159 ± 11 cm. The average track length is found to be 35.3 ± 2.5 cm.

We have scanned 86,498 frames of bubble chamber film in this experiment. The average number of beam tracks per frame is found to be 3.42 ± 0.20 . Thus, the total beam track length is $(10.44 \pm 0.95) \times 10^6$ cm. Using a value of 0.415 gm/cm^3 for the density of propane, the production cross-section is calculated to be 2.33 ± 0.36 mb. This value is consistent with the existing results from other similar experiments: 1.9 ± 0.5 mb at 850 MeV/c, 3.1 ± 0.5 mb at 1150 MeV/c, 2.2 ± 0.2 mb at 1220 MeV/c, and 1.4 ± 0.3 mb at 1510 MeV/c.

Production Angular Distribution

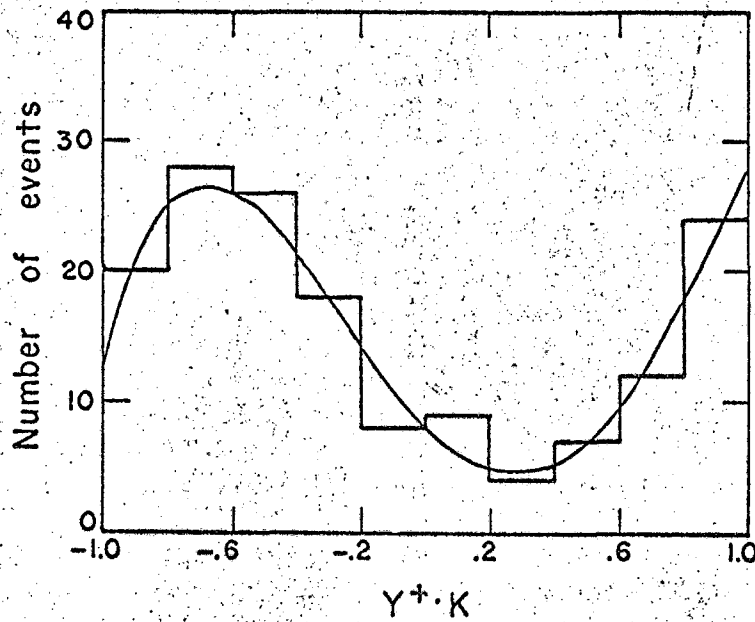
The distributions of cosine of the production angle, θ , are given in Figs. 12, and 13 for both the Y_1^{*+} and the Y_1^{*-} production, where θ is the angle between the incoming K^- and the outgoing Y_1^* directions in the center of mass of the K^-p system. They were both fitted to polynomials in $\cos \theta$. *

$$f(\theta) = \sum_n a_n \cos^n \theta$$

Table III shows the coefficients, a_n , for the best fitting polynomials.

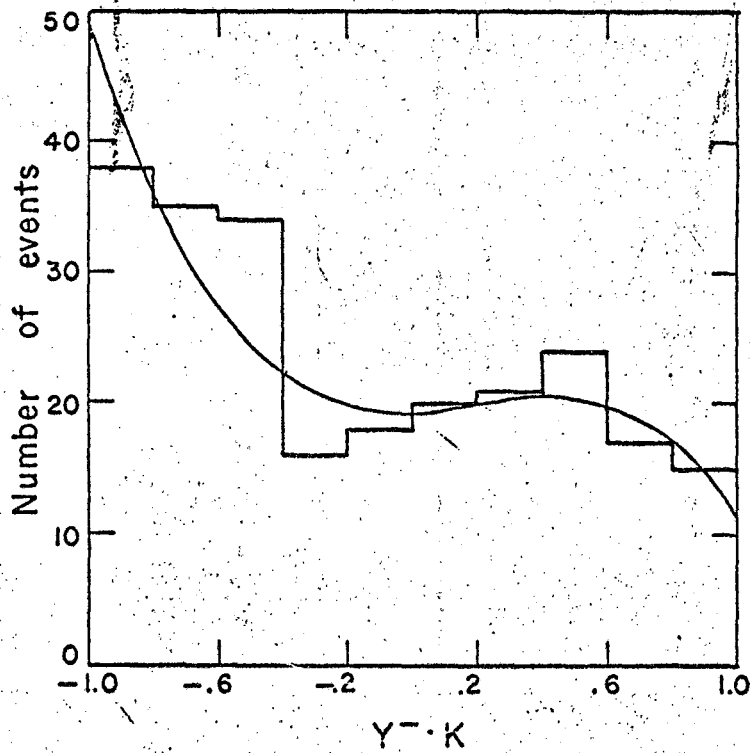
The two distributions are different. For the Y_1^{*+} , the fourth order term is necessary, for the Y_1^{*-} , a third order term. The addition of higher order terms did not improve the fits. The presence of both even and odd terms, and of terms higher than the second order indicates that the production was not in any pure angular momentum state and that up to D-wave production was present.

* All polynomial fittings were done by an IBM 704 program, PALSI (20)



MU-31653

Fig. 12. Distribution of $Y_1^+ \cdot K$, the cosine of production angle of Y_1^+ in the K^-p center of mass. Solid line is the best fitted polynomial in $Y_1^+ \cdot K$.



MU-31654

Fig. 13. Distribution of $Y \cdot K$, the cosine of production angle of Y^* in the K^-p center of mass. Solid line is the best fitted polynomial in $Y \cdot K$.

TABLE III

The coefficients of the polynomials in $\cos \theta$
fitted to the production angular distribution

	Y_1^{*+}	Y_1^{*-}
a_0	7.97 ± 1.79	19.5 ± 2.1
a_1	$-(25.86 \pm 5.25)$	0.6 ± 6.8
a_2	36.24 ± 15.2	11.1 ± 5.2
a_3	33.39 ± 8.74	$-(19.4 \pm 10.8)$
a_4	$-(23.77 \pm 19.2)$	

Decay Distribution of Y_1^*

The decay distribution in the Y_1^* center of mass frame depends strongly on whether the Y_1^* is produced and decays as a free particle. Unless the Y_1^* is in a free state, there will be interference effects due to (1) the Y_1^* and the background non-resonant $\Lambda \pi^- \pi^+$ productions, (2) the Y_1^{*+} and the Y_1^{*-} channels. These interference effects cause distortion in various angular distributions. Since the Y_1^* breaks up via strong decay, where parity is expected to be conserved, only even or odd partial wave states, but not both, can be present. The decay angular distribution of the lambda with respect to the Y_1^* direction in the Y_1^* center of mass frame would, therefore, display no fore-aft asymmetry. If it were fitted to a polynomial in $\cos \theta_{\Lambda Y}$, coefficients for the odd power terms should vanish.

Fig. 14 and 15 give the decay distributions for the Y_1^{*+} and the Y_1^{*-} respectively. In scanning we missed slow lambdas, the decay protons of which had too little energy to leave visible tracks. These were lambdas going forward in the Y_1^* center of mass frame. (See section 7 on cross-section corrections.) Thus, we left out the data $0.8 \leq \cos \theta_{\Lambda Y} \leq 1.0$ and fitted the rest with a distribution of the form

$$1 + a \cos \theta_{\Lambda Y}$$

as indicated by the solid curves. The coefficients are

$$a_+ = -(0.25 \pm 0.16) \text{ for } Y_1^{*+}$$

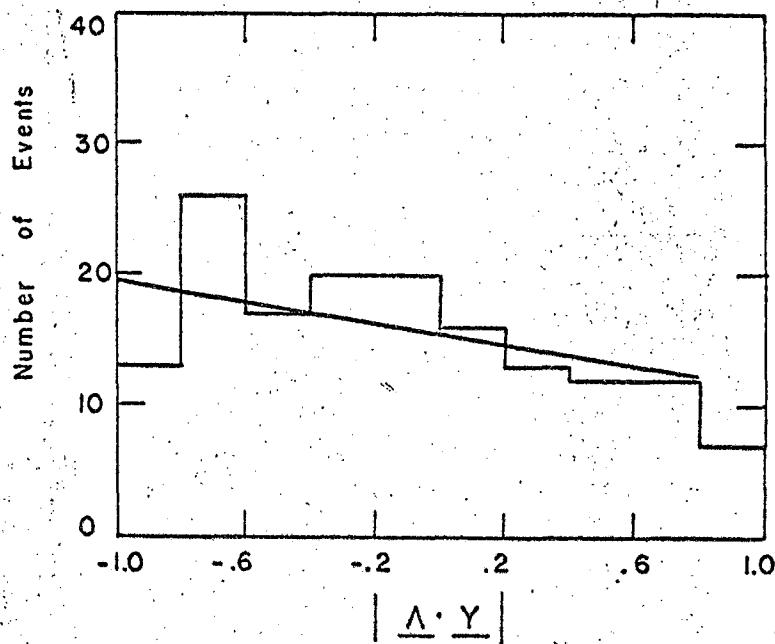
$$a_- = -(0.17 \pm 0.15) \text{ for } Y_1^{*-}$$

For the same interaction at 850 MeV/c⁽²¹⁾, where interference effects between the Y_1^{*+} and the Y_1^{*-} channels are strong, the coefficients were

$$a_+ = -(0.92 \pm 0.26)$$

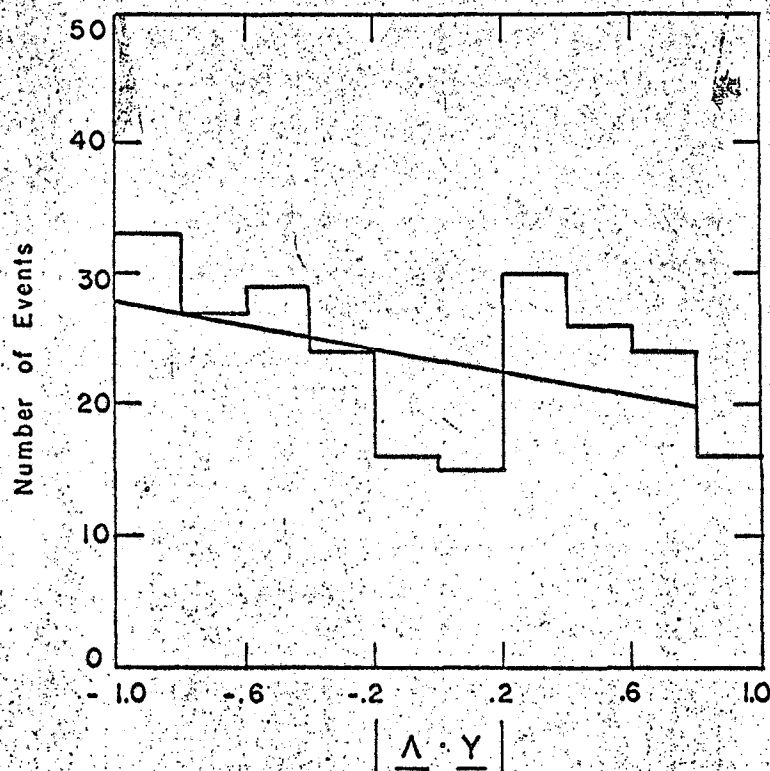
$$a_- = -(0.24 \pm 0.24)$$

Thus, it is reasonable to assume that, at the present energy, the Y_1^* was produced and decayed as a relatively free particle and the spin analyses are based on this assumption.



MU-31646

Fig. 14. Distribution of $\underline{\Delta} \cdot \underline{\Upsilon}$. The solid line is the best $1 + a(\underline{\Delta} \cdot \underline{\Upsilon})$ fit.



MU-31645

Fig. 15. Distribution of $|\underline{\Lambda} \cdot \underline{Y}|$. The solid line is the best $1 + a(\underline{\Lambda} \cdot \underline{Y})$ fit.

Spin Analysis

The spin state of Y_1^* can be manifested through its decay distributions. The lambda has a spin of $1/2$, and orbital angular momentum quantum numbers are integers. Thus, the spin of Y_1^* , J , must be half integer, i.e., $(2n + 1)/2$.

If J is $1/2$, there is no possible alignment of Y_1^* spin and the momentum vector of the decaying lambda, $\underline{\Lambda}$, in the Y_1^* center of mass must be isotropically distributed. If J is greater than $1/2$, it is possible to achieve an alignment of Y_1^* spin in the production process, which will in turn produce an anisotropy in the distribution of $\underline{\Lambda}$ about the axis of alignment.

A. Adair Analysis

Adair⁽²²⁾ has pointed out that for $J > 1/2$ the conservation of components of angular momentum along the incoming K^- beam direction (call this the z direction) forces the alignment of spin of those Y_1^* which are produced along or against this direction.

In the center of mass of the K^-p system along the z direction, the component of orbital angular momentum is zero. Since K^- has zero spin, only the spin of target proton contributes an angular momentum component of one-half. In the final interaction, the primary pion has spin zero and the orbital angular momentum of the Y_1^* which is produced either forward or backward with reference to the z axis has zero component along this direction. Thus, from conservation of momentum, the spin of Y_1^* must be aligned to give a z -component of $1/2$. For example, for $J = 3/2$, the $J_z = 3/2$ states are not allowed. Consequently, when $J > 1/2$, the distribution of $\underline{\Lambda.K}$ is anisotropic, where $\underline{\Lambda}$ is measured in the Y_1^* center of mass

and \underline{K} is measured in the center of the $K^- - p$ system. For $J = 3/2$, the distribution is of the form $1 + 3 (\underline{\Lambda} \cdot \underline{K})^2$. For $J = 5/2$, it is $1 - 2 (\underline{\Lambda} \cdot \underline{K})^2 + 5 (\underline{\Lambda} \cdot \underline{K})^4$.

However, there were few events that had Y_1^* produced exactly along the beam direction. Thus, we must also accept events that had production angle of Y_1^* close to but not equal to zero. The choice of cut-off of production angle depends on the production angular momentum state. If there were only s-wave state present, all events could be used. If higher partial wave states were present, the accepted production angle must be limited to $(L_{\max} + 1)^{-1}$ radians⁽²³⁾, where L_{\max} is the highest angular momentum state. As a result, the anisotropy would become less pronounced also.

For d-wave production, the production angle cut-off was limited to 0.33 radians about the beam direction, the cosine of which is 0.94. However, with this restricted cut-off, the data yielded too few events to be useful. Thus, we extended the cut-off to 0.9, corresponding to about 0.45 radian.

The decay distributions change when we allow events with production angles other than zero. Since the production angular distributions show that the Y_1^* production was not a pure state from their asymmetries, it is not clear what the expected decay distributions should be.

For example, in the case of the d-wave production of a $J = 3/2$ Y_1^* , if the total angular momentum of the final $\pi - Y_1^*$ configuration is $5/2$, the expected decay distribution average over $|\cos \theta_{\text{prod}}| > 0.9$ is $1 + 7 (\underline{\Lambda} \cdot \underline{K})^2$.

Since only the even power terms of $(\underline{\Lambda} \cdot \underline{K})$ appear in the expected

distributions, we folded the $(\underline{\Lambda} \cdot \underline{K})$ distribution along $\underline{\Lambda} \cdot \underline{K} = 0$. Fig. 16 shows the distribution of both the Y_1^{*+} and the Y_1^{*-} events with $1305 < M_{\Lambda\pi} < 1445$ MeV and $|\cos \theta_{\text{prod}}| > 0.9$. There were 44 events. The solid line is the best fitted distribution of the form

$$1 + a (\underline{\Lambda} \cdot \underline{K})^2$$

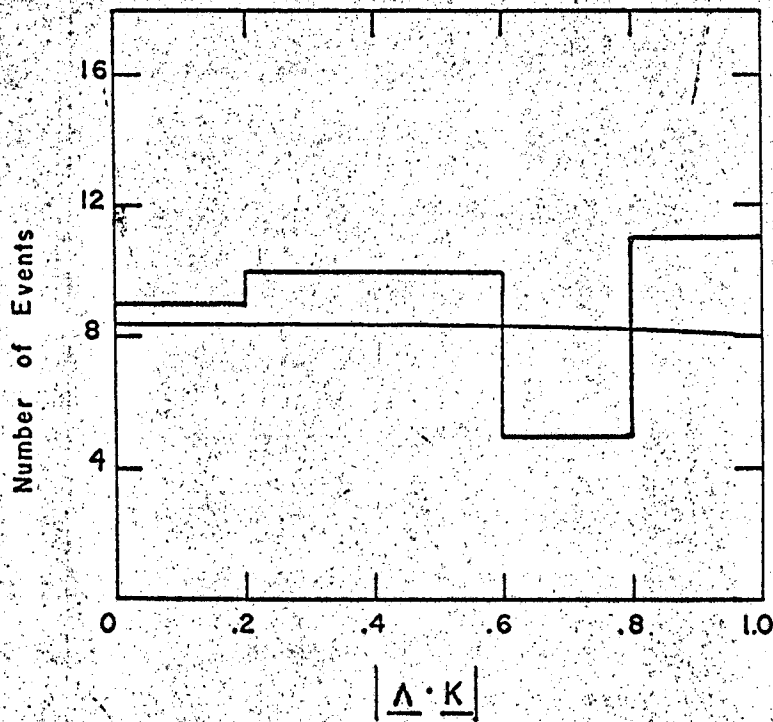
where $a = -(0.05 \pm 0.66)$. The distribution agrees very well with isotropy.

With a narrow $M_{\Lambda\pi}$ cut-off, $1345 < M_{\Lambda\pi} < 1425$ MeV, $a = -(0.25 \pm 0.66)$. The distribution again is consistent with isotropy.

B. Decay distribution with respect to the production normal

If any Y_1^* decay distribution is found to be non-isotropic, assuming there is no strong interference to distort this distribution, this would exclude the possibility that the spin of Y_1^* is $1/2$.

We had studied the distribution of $\underline{\Lambda} \cdot \underline{n}$, where \underline{n} is the production normal, defined as $\underline{K} \times \underline{Y}$, both being unit vectors in the center of mass of K^-p system, and $\underline{\Lambda}$ is defined in the Y_1^* center of mass. For those Y_1^* 's that were produced close to the beam direction, the normal \underline{n} was not well defined experimentally. Thus, we restricted our analysis to those events where $|\cos \theta_{\text{prod}}| < 0.5$. These distributions involve a different sample of events than those in the Adair analysis and include both the Y_1^{*+} and the Y_1^{*-} events. They are non-isotropic, the lambdas were emitted preferentially perpendicular to the production plane containing the Y_1^* and the K^- in the center of mass of the K^-p system. When the $\underline{\Lambda} \cdot \underline{n}$ distributions were fitted with a power series in $(\underline{\Lambda} \cdot \underline{n})$, the coefficients for the linear term are small compared with those for the quadratic



MU-31649

Fig. 16. Distribution of $|\underline{\Lambda} \cdot \underline{K}|$ for both the γ^{*+} and the γ^{*-} . The solid line is the best fit of the form $1 + a(\underline{\Lambda} \cdot \underline{K})^2$.

term and all the high power terms other than the quadratic do not improve the fitting. The results for two invariant mass intervals, $M_{\Lambda\pi}$, are tabulated as follows:

Decay Distribution

$$\begin{array}{ll} 1305 < M < 1445 \text{ MeV} & 1 - (0.40 \pm 0.27) (\underline{\Lambda.n}) + (2.18 \pm 0.55) (\underline{\Lambda.n})^2 \\ 1345 < M < 1425 \text{ MeV} & 1 - (0.39 \pm 0.31) (\underline{\Lambda.n}) + (2.21 \pm 0.63) (\underline{\Lambda.n})^2 \end{array}$$

Noting the relative small value of linear term coefficients, the distributions were folded and fitted to a curve of the form $1 + a (\underline{\Lambda.n})^2$ as shown in Fig. 17. The distributions are more than three standard deviations from isotropy. And the values of a obtained are

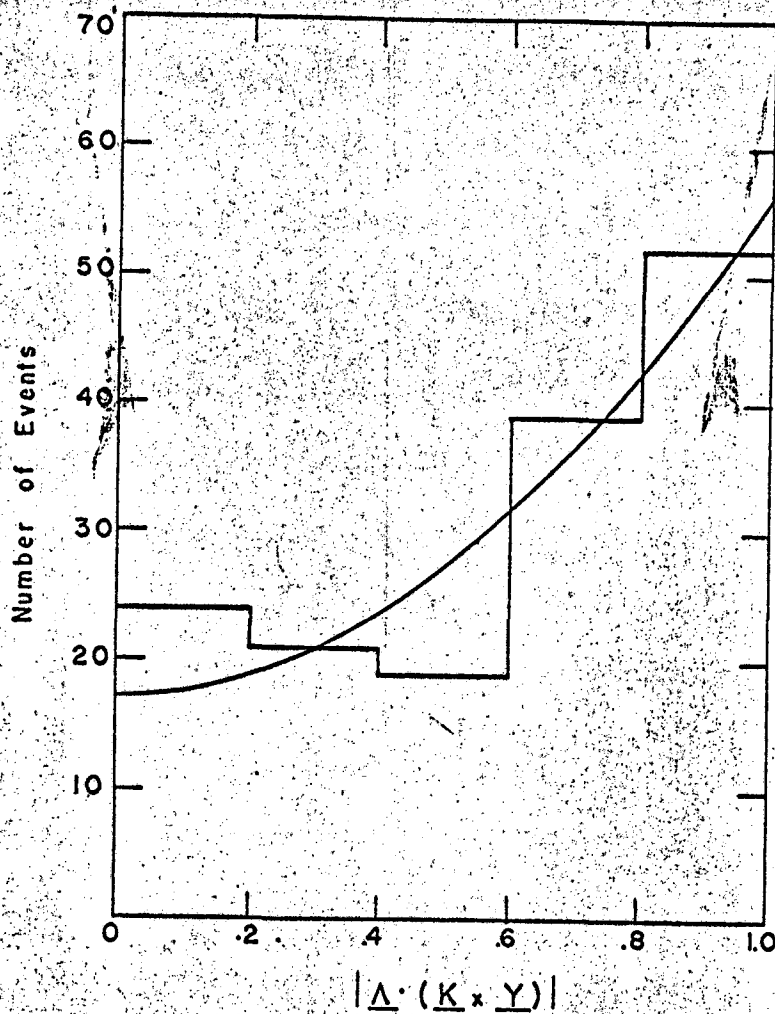
$$1305 < M_{\Lambda\pi} < 1445 \text{ MeV: } a = 2.21 \pm 0.56$$

$$1345 < M_{\Lambda\pi} < 1425 \text{ MeV: } a = 2.03 \pm 0.62$$

This anisotropy persisted when we studied the Y_1^{*+} and the Y_1^{*-} samples separately.

Fig. 18 shows the decay distribution, $\underline{\Lambda.n}$, for four invariant mass intervals: (a) $1355 < M_{\Lambda\pi} < 1370$ MeV, (b) $1370 < M_{\Lambda\pi} < 1385$ MeV, (c) $1385 < M_{\Lambda\pi} < 1400$ MeV, (d) $1400 < M_{\Lambda\pi} < 1415$ MeV. The statistics are poor. Except for the last interval, the anisotropy persists and there is no indication that the angular distributions vary strongly as the value of the invariant mass passes through resonance.

The anisotropy in the decay distribution and its persistence can be simply explained by the high spin of the Y_1^* . In other words, the Y_1^* alone with its spin equal to $1/2$ cannot produce an anisotropic decay distribution. However, Adair⁽²⁴⁾ shows that if one allows

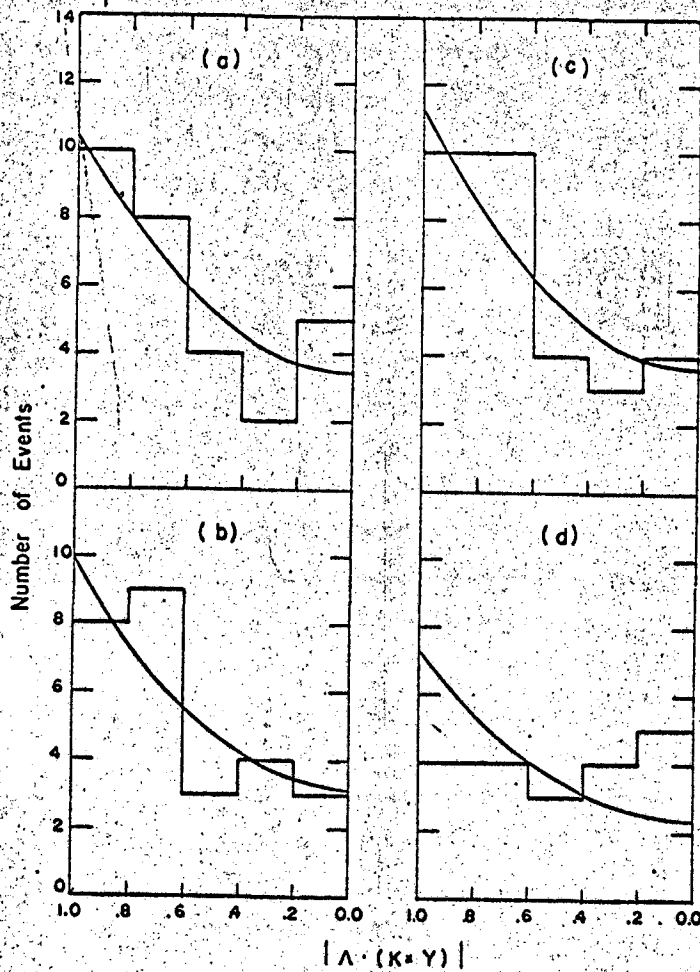


MU.31648

Fig. 17. Distribution of $|\underline{\Lambda} \cdot (\underline{Y} \times \underline{K})|$. The solid line is the best fitted curve of the form $1 + a(\underline{\Lambda} \cdot \underline{Y} \times \underline{K})^2$.

for a non-resonant background which is coherent with the resonant amplitude, the resulting interference can give appreciable anisotropies. Thus, even if the spin were $1/2$, with a 8% non-resonant background intensity, the interference would produce an anisotropic distribution of the form $1 + a \cos^2 \theta$ with $a = 2.0$. Adair further shows that the variation of anisotropy needs not be large as the value of the invariant mass passes through resonance.

Thus, the existence of anisotropy in the decay distribution can be explained by (1) a simpler hypothesis that the spin of the Y_1^* is equal to or greater than $3/2$, or (2) a spin $1/2$ hypothesis with specifically definite phase relations between the eigenstates of the resonance and the background.



NY-31647

Fig. 18. Distribution of $|\Lambda \cdot (\underline{Y} \times \underline{K})|$ as a function of $M_{\pi\Lambda}$.

Polarization of Lambdas

An analysis of the average polarization of lambdas, \bar{P} , may yield information with regard to the relative parity of the $Y_1^* - \Lambda$ system.

The distribution of θ was studied, where θ is the angle between the proton from lambda decay and the Y_1^* production normal. If we denote by N_{up} the number of decays having $\cos \theta > 0$, then

$$\alpha \bar{P} = \frac{N_{up} - N_{down}}{1/2 (N_{up} + N_{down})}$$

where α is the asymmetry coefficient of Λ , equal to 0.67 ± 0.07 (25). Assuming the Y_1^* has a spin of $3/2$, for D-wave decay, $|\bar{P}| = 2/5 |P_{Y^*}|$; for a P-wave decay, $|\bar{P}| = 2/3 |P_{Y^*}|$. P_{Y^*} is the average polarization of the Y_1^* .

For the events in the mass interval 1345 - 1425 MeV, the values of \bar{P} found for two production angle intervals are given in Table IV, $0 \leq \cos \theta \text{ prod} \leq 1$ and $0 \leq \cos \theta \text{ prod} \leq 0.75$. From the results of the combined data of both the Y_1^{*+} and Y_1^{*-} , we cannot make any conclusion as to the relative parity of the $Y_1^* - \Lambda$ system. We also studied the polarization of lambda from the Y_1^{*-} and the Y_1^{*+} separately. The data from Y_1^{*-} gave no polarization. Those from the Y_1^{*+} yielded a large value, 0.75 ± 0.33 . Since the maximum value of P_{Y^*} possible is unity, the maximum value of the polarization of lambdas, \bar{P} , is generally less than 0.4 for a D-wave decay, and less than 0.66 for a P-wave decay. Thus, while all the values for \bar{P} are compatible with both hypotheses, the large polarization in the Y_1^{*+} sample agrees better with the P-wave or even parity case.

TABLE IV
Average polarization of lambda from Y_1^* decay

	$\cos \theta_{\text{prod}}$	$d\bar{P}$	\bar{P}
Y_1^{*0}	< 0.75	$.26 \pm .13$	$.39 \pm .21$
	< 1.0	$.22 \pm .11$	$.33 \pm .18$
Y_1^{*+}	< 0.75	$.50 \pm .21$	$.75 \pm .33$
	< 1.0	$.41 \pm .17$	$.61 \pm .27$
Y_1^{*-}	< 0.75	$.10 \pm .17$	$.15 \pm .26$
	< 1.0	$.09 \pm .15$	$.13 \pm .23$

Results and Conclusions

From the study of the invariant mass between the lambda and the pions in the final state, we have found that the ratio of cross-sections for producing Y_1^{*-} 's and Y_1^{*+} 's is not unity. The total isotopic spin state of the final $\Lambda \pi^- \pi^+$ system is a mixture of $I = 0$ and $I = 1$ states. If the final state were reached by either one of the isotopic spin channels, then the cross-section ratio would be unity.

That the production was not via a single isotopic spin channel is further borne out by the difference in the Y_1^{*-} and the Y_1^{*+} production angular distribution. We also observed a difference in mass-width between their mass peaks. All these effects were presumably due to the interference of the $I = 0$ and the $I = 1$ amplitudes.

It is interesting to note that if we limit the maximum allowed production angular momentum state to D-wave, then the only pure $\pi - Y_1^*$ configuration which will reproduce a large negative $\cos^4 \theta$ term in the production angular distribution is $(d P_{3/2})_{5/2}$. That is a D-wave production of a spin $3/2$ Y_1^* via an intermediate state having total angular momentum of $5/2$. We are in no way maintaining that this is the exclusive evidence for the spin of Y^* being $3/2$.

Rather, the conclusion of the spin of Y_1^* being $3/2$ is based upon the anisotropy of the lambda decay distributions measured with respect to the production normal.

In the Adair analysis for determination of the spin, we were hampered by poor statistics. In order to gain more events, we had to accept events with Y_1^* 's produced farther away from the beam direction. But in doing so, the advantage of the Adair analysis,

that the distribution does not depend upon the production mechanism, was no longer accessible. Not only the expected anisotropy, if J is greater than one-half, became less pronounced, but also, because we were not certain of the exact production partial waves, the expected Adair decay distribution became obscure. Thus, we have not gained any additional knowledge in the present Adair analysis.

The anisotropy in the lambda decay distribution with respect to the production normal is quite pronounced. It persists throughout the data whether we used all events or only those within certain mass intervals. It persists as we vary the mass intervals from one side of the peak of the resonance to the other side. Had the anisotropy been due to background interference, the background would have to be of definite composition and of specific phase. The presence of negligible asymmetry in the lambda decay distribution with respect to the Y_1^* direction is also observed in the sample of events used in the spin analysis. This validates the assumption that the Y_1^* resonance was produced and decayed as a relatively free particle in the present interaction. All these indicate that the anisotropy obtained is real, and leads to the conclusion that the spin of Y_1^* is equal to or greater than $3/2$.

All the above results favor a value of $3/2$ for the spin of the Y_1^* . But they can be reproduced by introducing specific background interferences to a spin $1/2$ Y_1^* . In order to determine the spin unambiguously, a series of experiments, done at various energies, is in order where a detailed study of the production and the decay distributions with good statistics can be undertaken.

Acknowledgments

I would like to thank Professor Wilson M. Powell for his guidance throughout my graduate studies and for his suggestion of this experiment.

I am greatly indebted to Drs. Robert W. Birge, Robert P. Ely, Jr., and George Gidal for their constant advice and counsel.

Helpful discussions with Dr. Albert Werbrouck, Dr. Peter Newcomb, Mr. Yu-Li Pan and Mr. Thomas Schumann are greatly appreciated.

Dr. Peter Newcomb did the beam momentum analysis. Mr. Thomas Schumann scanned the film for delta rays. Mr. Yu-Li Pan contributed immensely in analyzing the data.

Mrs. Mattie L. Woodford did most of the scanning.

The cooperation of Mr. Paul Weber and his data processing section is invaluable.

The assistance of Mr. Howard White and his data handling group is gratefully acknowledged.

The cooperation of the Bevatron crew under the direction of Dr. Edward Lofgren, and of the bubble-chamber crew under the direction of Mr. Larry Oswald is indispensable.

In preparing this manuscript, the efforts of the following persons are acknowledged with pleasure: Miss Kathy Tennant, Miss Charlotte Scales, Mrs. Marleigh Sheaf, Mrs. Nancy Wakeman.

And last, but not least, to each and every member of the Powell-Birge group, past and present, my heartfelt thanks.

This work was done under the auspices of the U. S. Atomic Energy Commission.

References

1. W. M. Powell, W. B. Fowler, and L. O. Oswald, Rev. Sci. Instr. 29, 874 (1958)
2. P. Eberhard, M. L. Good, and H. K. Ticho, Rev. Sci. Instr. 31, 1054 (1960)
3. M. Alston, L. W. Alvarez, P. Eberhard, M. L. Good, W. Graziano, H. K. Ticho, and S. G. Wojcicki, Phys. Rev. Letters 5, 520 (1960)
4. M. Gell-Mann, Phys. Rev. 106, 1296 (1957)
5. R. H. Dalitz and S. F. Tuan, Phys. Rev. Letters 2, 425 (1959)
R. H. Dalitz, Phys. Rev. Letters 6, 239 (1961)
6. L. T. Kerth and A. Pais, On the Gentle Art of Hunting Bumps, UCRL-9706, May 19, 1961
7. L. W. Alvarez in 9th International Annual Conference on High Energy Phys., Kiev, 1959 (Academy of Sciences (IUPAP), Moscow, Russia, 1960), 2 vols.
8. W. E. Humphrey, Hyperon Production by K^- Mesons Incident on Hydrogen (thesis), UCRL-9752, June 12, 1961 (unpublished)
R. Ross, Elastic and Charge Exchange Scattering of K^- Mesons in Hydrogen (thesis), UCRL-9749, June 21, 1961 (unpublished)
9. P. Newcomb, Experiment No. 16 Beam Momentum (Intergroup report)
10. M. Roos, Rev. Mod. Phys., 35, 314 (1963)
11. J. Shonle, Differential Elastic Pion-Proton Scattering at 600,650 and 750 MeV (thesis), UCRL-9362, August 12, 1960
12. H. S. White, Identification Curves for Heavy-meson and Hyperon Decays, UCRL-3514, Sept. 19, 1956
13. Reference Manuals. FOG CLOUDY FAIR Bubble Chamber Data Processing System. Lawrence Radiation Laboratory Document UCID 1340 (unpublished)

14. J. Button and A. Rosenfeld, "Probability Paper" for Testing Chi-squared Distributions, UCRL Physics Note Memo 240, Dec. 14, 1960
15. M. Horovitz, IBM Program Athos -- Phase Space Calculations, UCRL Internal Report, Physics Note 394, May 1962 (unpublished)
16. M. Gell-Mann and A. Rosenfeld, Ann. Rev. Nuc. Sci., 7, 407 (1957)
17. G. A. Snow and M. M. Shapiro, Rev. Mod. Phys., 33, 231 (1961)
18. S. Y. Fung, Bull. Amer. Phys. Soc., 7, 619 (1962)
19. L. T. Kerth, Rev. Mod. Phys., 33, 389 (1961)
20. R. E. von Holdt, PALSI-A Polynomial Approximating Code, Lawrence Radiation Laboratory Report UCRL 10478, Sept. 1962 (unpublished)
21. J. P. Berge, P. Bastien, O. Dahl, M. Ferro-Luzzi, J. Kirz, D. H. Miller, J. J. Murray, A. H. Rosenfeld, R. D. Tripp, and M. B. Watson, Phys. Rev. Letters, 6, 557 (1961)
22. R. K. Adair, Phys. Rev., 100, 1540 (1955)
23. R. H. Dalitz, Brookhaven National Laboratory Report, BNL 735 (T-264) (unpublished)
24. R. K. Adair, CERN/TC/PHYSICS 63-12, (to be published in Phys. Review)
25. J. W. Cronin and D. E. Overseth, International Conference on High-Energy Nuclear Physics at CERN, 1962

This report was prepared as an account of Government sponsored work. Neither the United States, nor the Commission, nor any person acting on behalf of the Commission:

- A. Makes any warranty or representation, expressed or implied, with respect to the accuracy, completeness, or usefulness of the information contained in this report, or that the use of any information, apparatus, method, or process disclosed in this report may not infringe privately owned rights; or
- B. Assumes any liabilities with respect to the use of, or for damages resulting from the use of any information, apparatus, method, or process disclosed in this report.

As used in the above, "person acting on behalf of the Commission" includes any employee or contractor of the Commission, or employee of such contractor, to the extent that such employee or contractor of the Commission, or employee of such contractor prepares, disseminates, or provides access to, any information pursuant to his employment or contract with the Commission, or his employment with such contractor.

